International Journal of Thermophysics, Vol. 27, No. 2, March 2006 (© 2006)
DOI: 10.1007/s10765-006-0058-x

Transient Coupled Heat Transfer in Multilayer Non-gray Semitransparent Media with Reflective Foils

Dan Bai[1,2] **and Xu-Ji Fan**[1]

Received January 14, 2005

In this paper, transient coupled radiative and conductive heat transfer in multilayer thermal insulation (MTI), which consists of non-gray semitransparent materials and reflective foils, is investigated for re-entry aerodynamic heating. The governing equation for combined radiation and conduction heat transfer in MTI is solved using a finite volume numerical method, whereas the radiative transfer equation (RTE) is solved using a finite difference method, in which the spectral scattering and absorption coefficients are determined using the Mie theory and the scattering phase function is modeled by the Delta-Eddington approximation. A comparison is carried out between numerical results for coupled heat transfer in non-gray MTI and those obtained by the two-flux model in which the medium is assumed to be gray. Finally, the numerical optimization of MTI is discussed.

KEY WORDS: multilayer thermal insulation; non-gray semitransparent media; radiative transfer equation; reflective foils.

1. INTRODUCTION

To maintain appropriate temperatures for equipment, payloads, and structures during re-entry aerodynamic heating, an efficient thermal protection system (TPS) is required. Metallic thermal protection systems have been developed for intended use on major portions of reusable launch vehicles. The use of high temperature multilayer insulation in this kind of thermal protection system is investigated in the present study. The multilayer insulation consists of thin ceramic or composite foils with

[1] School of Mechanical Engineering, Shanghai Jiaotong University, Shanghai 200030, P. R. China.
[2] To whom correspondence should be addressed. E-mail: baidan1@sjtu.edu.cn

a high reflectance metal coating separated by fibrous insulation spacers as described in Ref. 1. The fibrous insulation spacers are made of a low-density, low-thermal-conductivity material, such as high-purity silica fiber, high-purity alumina fiber [2, 3], etc.

Heat transfer in multilayer insulation involves combined modes of heat transfer: solid conduction through fibers, gas conduction and natural convection in spaces between fibers, and radiation interchange in the fibrous insulation. In the present study gas natural convection was not considered. As most of the materials that exchange heat by means of radiation are non-gray, one must take into account the wavelength dependence. The radiative properties (the complex optical index or emissivity) of non-gray media vary with wavelength, while those of gray media are independent of wavelength. In this context the term gray is employed to connote the fact that the material is completely nonselective in its spectral characteristics. There are very few materials for which the emissivity is constant over the entire range of wavelengths. In spite of this fact, many materials can be considered to be approximately gray bodies. However, materials, which exchange heat by means of radiation in high-temperature multilayer insulation with reflective foils need to be more accurately characterized because radiation is significant at high temperatures. The situation described above not only contributes to the design for TPS but also to the choice of materials for TPS. The appropriate design and use of high-performance materials will enhance the payload of reusable launch vehicles. In fact, a series of the effects on the design for TPS, caused by the assumption in which a non-gray material is considered to be an approximately gray material, is also of interest to most engineers.

The objective of this paper is to compare the numerical results obtained for non-gray fibrous insulation with those obtained for fibrous insulation assumed as gray material by the use of appropriate numerical heat transfer models. Modeling for non-gray media is characterized by solving the radiative transfer equation (RTE), while the modeling for gray media is characterized by the two-flux approximation.

2. DESCRITPION OF MULTILAYER INSULATION FOR RE-ENTRY AERODYNAMIC HEATING

In this study the investigated multilayer insulation consisted of reflective foils separated by layers of silica fibrous insulation. It had five $304.8\,\text{mm} \times 304.8\,\text{mm} \times 0.0404\,\text{mm}$ gold-coated foils with a density of $1343\,\text{kg} \cdot \text{m}^{-3}$. The four interior fibrous insulation spacers were 3.78 mm thick with a density of $20\,\text{kg} \cdot \text{m}^{-3}$, while the two outer fibrous insulation

spacers were 1.80 mm thick with the same density. The height of the insulation sample, combined foils and spacers, was 18.92 mm. The multilayer insulation was wrapped in a 0.43 mm thick Nextel bag. A schematic of the multilayer sample is shown in Fig. 1.

The fibrous insulation spacers were made of randomly oriented silica fibers with a diameter of 7 μm. The typical values of n_λ and k_λ for silica are presented in Ref. 4 and described in Fig. 2. From Fig. 2, the variation of the optical properties of silica fibers with wavelength showed that the silica fibrous insulation is non-gray.

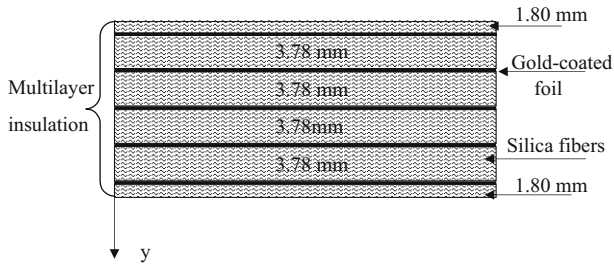

Fig. 1. Schematic of the multilayer insulation.

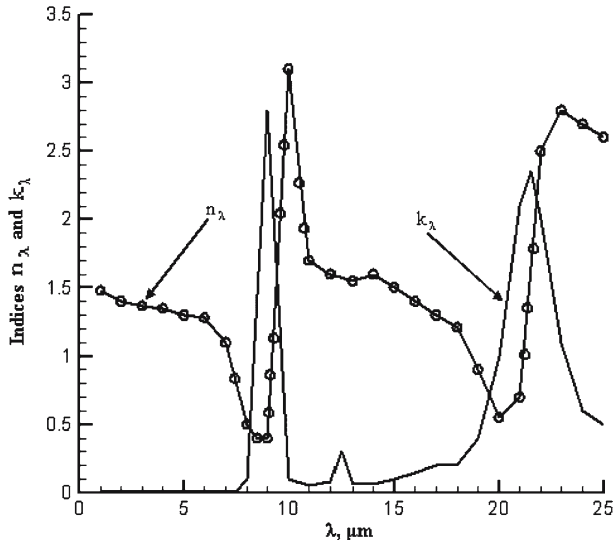

Fig. 2. Silica optical properties.

3. HEAT TRANSFER MODEL

The governing conservation of energy equation for the problem of combined radiation and conduction in a radiation participating media with a thickness E bounded by two solid surfaces at specified temperatures is given by [5]

$$\rho C_p \frac{\partial T(y,t)}{\partial t} - \frac{\partial}{\partial y}\left(k\left(T\left(y,t\right)\right)\frac{\partial T(y,t)}{\partial y}\right) = S_r\left(y,t\right) \tag{1}$$

$$S_r\left(y,t\right) = -\frac{\partial Q_r(y,t)}{\partial y} \tag{2}$$

subject to the following initial and boundary conditions:

$$T(y,0) = T_{\mathrm{o}} \tag{3}$$

$$T(0,t) = T_1(t) \tag{4}$$

$$T(E,t) = T_2(t) \tag{5}$$

where T is the temperature, ρ is the density, C_P is the specific heat, $k(T)$ is the thermal conductivity, $S_{\mathrm{r}}(y,t)$ is the radiative source term, $Q_{\mathrm{r}}(y,t)$ is the radiant heat flux, t is the time, and y is the spatial coordinate through the insulation thickness. For this application, $\rho = 20\,\mathrm{kg}\cdot\mathrm{m}^{-3}$ and $C_P = 670\,\mathrm{J}\cdot\mathrm{kg}^{-1}\cdot\mathrm{K}^{-1}$.

The radiant heat flux is given by

$$Q_{\mathrm{r}}\left(y,t\right) = 2\pi \int_{\lambda=0}^{\infty} \int_{\mu=-1}^{1} I_\lambda\left(y,\mu,t\right)\mu \mathrm{d}\mu \mathrm{d}\lambda \tag{6}$$

and $I_\lambda(y,\mu,t)$ is determined from RTE as described below. The conductive heat flux is defined by

$$Q_c(y,t) = -k(T(y,t))\frac{dT(y,t)}{dy} \quad \forall 0 < y < E \tag{7}$$

In Eqs. (1) and (7), $k(T)$ is the thermal conductivity which depends on temperature. The function of the thermal conductivity of fibrous insulation made up of the silica fibers and air is derived using the Langlais and Klarsfeld semi-empirical relation [6].

$$k(T) = 2.572\times10^{-4}T^{0.81} + 5.27\times10^{-5}\rho^{0.91}(1 + 1.3\times10^{-3}T) \tag{8}$$

where T is the temperature and ρ is the density of the fibrous insulation, which is $20\,\mathrm{kg}\cdot\mathrm{m}^{-3}$ in this study. This relation corresponds to the

heat transfer through the thickness of the insulator and takes into account the air and glass fiber conduction as well as contacts between fibers. The validity range of this relation is for temperatures from approximately 273 to 1000 K. This relation is used over the entire temperature range in the present application.

The total heat flux is given by the sum of radiative and conductive heat fluxes,

$$Q_{\mathrm{t}}(y,t) = Q_{\mathrm{c}}(y,t) + Q_{\mathrm{r}}(y,t) \tag{9}$$

For a non-grey absorbing, emitting, and anisotropic scattering medium of thickness E, assuming heat transfer in the y-direction, with an axial symmetry, the RTE [7] is described as

$$\begin{aligned}\frac{1}{c}\frac{\partial I_\lambda(y,\mu,t)}{\partial t} + \mu\frac{\partial I_\lambda(y,\mu,t)}{\partial y} &= -\beta_\lambda(\mu)\, I_\lambda(y,\mu,t) + \sigma_{a\lambda}(\mu)\, I_{b,\lambda}(T(y,t)) \\ &\quad + \frac{1}{2}\int_{\mu'=-1}^{1} \sigma_{s\lambda}(\mu')\, \Phi_\lambda(\mu' \to \mu) I_\lambda(y,\mu',t)\, d\mu'\end{aligned} \tag{10}$$

for all $0 < y < E$, $\mu \in [-1, 0) \cup (0, 1]$, $\lambda > 0$. The coefficient c is the velocity of light in the medium of interest through which the radiation travels ($c = 2.998 \times 10^8\ \mathrm{m \cdot s^{-1}}$); thus, the term $1/c\partial I_\lambda(y,\mu,t)/\partial t$ in the equation can be neglected in comparison to other terms. The coefficient μ is the cosine of the polar angle between the direction of propagation and transfer. In Eq. (10), the terms on the right-hand side describe, respectively, the extinction phenomena, the internal emission, and the intensity of the scattering in the μ direction. $I_\lambda(y,\mu,t)$ is the monochromatic radiation intensity, and $I_{b,\lambda}(T(y,t))$ is the monochromatic intensity of the blackbody at the temperature T, given by Planck's law as

$$I_{b,\lambda}(T) = \frac{C_1}{\tilde{n}_\lambda^2 \cdot \lambda^5 \cdot \left[\exp\left(\frac{C_2}{\lambda \cdot \tilde{n}_\lambda \cdot T}\right) - 1\right]} \tag{11}$$

where C_1 and C_2 are two constants of radiation;

$$C_1 = 1.1910 \times 10^{-16}\ \mathrm{W \cdot m^2 \cdot sr^{-1}} \text{ and } C_2 = 1.4388 \times 10^{-2}\ \mathrm{m \cdot K}$$

The index of refraction $\tilde{n}_\lambda$ refers to the medium bounding the blackbody and is close to one ($\tilde{n}_\lambda \approx 1$). The investigated fibrous insulation is made of silica fibers and air with a preponderance of air. The silica density (ρ_{glass}) is equal to $2500\ \mathrm{kg \cdot m^{-3}}$, and the investigated fibrous insulation density

(ρ) is equal to $20\,\mathrm{kg}\cdot\mathrm{m}^{-3}$. Thus, the volume fraction $f_v = \rho/\rho_{\mathrm{glass}} = 0.008$; then, we can assume, for the investigated fibrous insulation, a refractive index of the bounding medium is close to one.
The monochromatic extinction coefficient is

$$\beta_\lambda = \sigma_{a\lambda} + \sigma_{s\lambda} \tag{12}$$

where the monochromatic absorption coefficient $\sigma_{a\lambda}$ and the monochromatic scattering coefficient $\sigma_{s\lambda}$ are cited in Ref. 5 (calculated results determined from the MIE theory) and described in Figs. 3 and 4. Wavelengths between 2.5 and $25\,\mu$m are considered in order to cover a temperature range between 1300 K and room temperature. Due to the highly forward scattering phase function of silica fiber, the scattering phase function is given by the Delta-Eddington approximation [2]:

$$\begin{aligned}\Phi_\lambda\left(\mu' \to \mu\right) &= 2f_\lambda \delta\left(1-\cos\theta\right) + \left(1-f_\lambda\right)\left(1+A\cos\theta\right) \\ &= 2f_\lambda \delta\left(1-\mu\right) + \left(1-f_\lambda\right)\left(1+A\mu\right)\end{aligned} \tag{13}$$

where $\delta(x)$ is the delta function and f_λ is the forward scatting factor. The modified scattering phase function of porous media is described through the reformulation approach developed by Joseph and Wiscombe [8]. Then the modified scattering phase function is given by $\Phi_\lambda\left(\mu' \to \mu\right) = 1 + A\mu$.

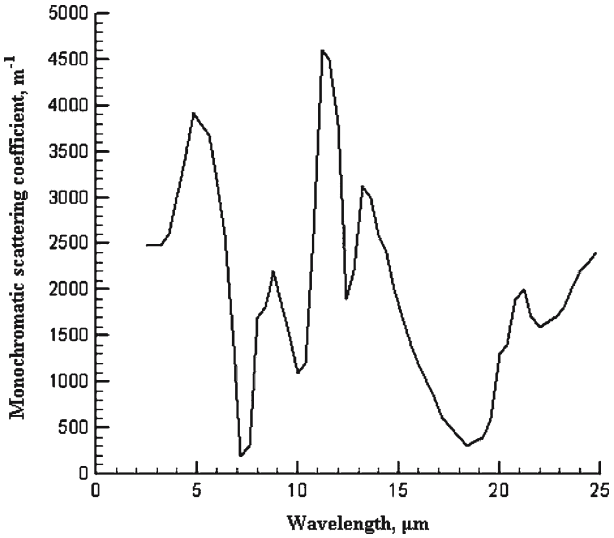

Fig. 3. Scattering coefficients versus wavelength.

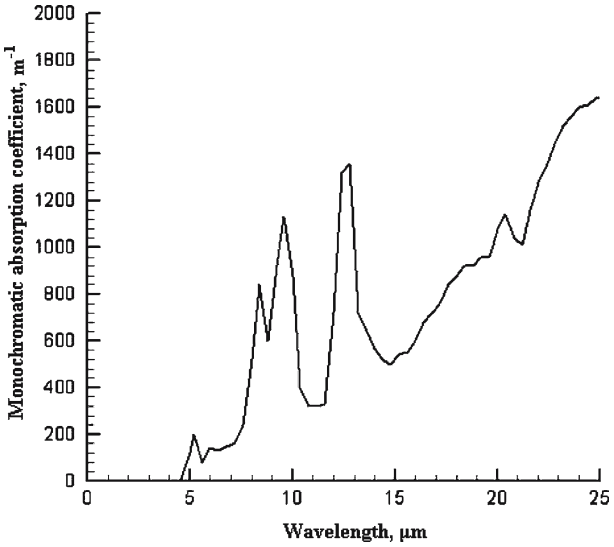

Fig. 4. Absorption coefficients versus wavelength.

The parameter A is nominally taken to be 1. A detailed explanation of this is given in Ref. 2.

In the MIE theory, the model applied for the determination of radiative properties of a medium depends on optical parameters (the complex optical index of fibers) and on morphological parameters (diameter and distribution of fibers, density of the medium). In other words, different materials that have different optical parameters will have different radiative properties from the MIE theory. As a consequence, different results are obtained. It should be mentioned that the real n_λ and imaginary k_λ parts of the complex index ($n_\lambda^* = n_\lambda - ik_\lambda$) depend on wavelength. The specific emissivity of the medium is similar to the complex optical index of the medium since both of them depend on the wavelength. From electromagnetic theory, the complex optical index is employed to denote the emissivity of the medium.

The monochromatic radiation intensity in each fibrous insulation spacer is obtained by solving Eq. (10), subject to the following boundary conditions at the bounding surfaces for the fibrous spacers, or at two foils or a foil and solid bounding surface [9, 10]:

$$I_\lambda(y_L, \mu, t) = \varepsilon_L I_{b,\lambda}(T_L(y_L, t)) + (1 - \varepsilon_L) I_{\lambda\,\mathrm{in}}(y_L, \mu, t) \quad \text{for} \quad 0 < \mu \leqslant 1 \tag{14}$$

$$I_\lambda(y_R, \mu, t) = \varepsilon_R I_{b,\lambda}(T_R(y_R, t)) + (1 - \varepsilon_R) I_{\lambda\,in}(y_R, \mu, t) \quad \text{for} \quad -1 \leqslant \mu < 0 \tag{15}$$

where ε is the emissivity of the foil or the solid bounding surface. The emissivity of the gold-coated foils has a constant value of 0.1 in the temperature range of 293 to 903 K [1], while the emissivity of the solid surface is equal to 0.8. These values were used throughout the entire temperature range. $I_{\lambda \text{in}}$ is the monochromatic incident radiation intensity, and the subscripts L and R refer to the fibrous spacers' two bounding surfaces. Equations (1) to (15) provide the governing equations and the most general form of the boundary conditions and initial conditions for the numerical heat transfer model. The assumption used at the boundary is as follows: the foil and solid bounding surface are opaque, diffuse emitting and reflecting. Another assumption is that the foil is isothermal since the foils are very thin in comparison to fibrous insulation spacers (the ratio of the thickness of the foil to the thickness of fibrous spacers is $0.0404/3.78 = 0.010$).

4. NUMERICAL SOLUTION OF HEAT TRANSFER MODEL

The overall solution scheme of the transient coupled equations is iterative. The flow chart of the algorithm is given in Fig. 5. First, we introduce the geometrical, thermal, and radiative data, and then we construct a mesh. Starting with the initial temperature field at a time $t = 0$, the solution of RTE Eq. (10) for each spacer region based on the finite difference method is calculated. The radiant heat flux variation Q_{r} and the radiative source term S_{r} are determined in each spacer region at the time $t = 0$, and then S_r is used in the governing conservation of energy Eq. (1) for obtaining the temperature distribution at succeeding times in the entire medium. In the following section, the solution of RTE and the conservation of energy equation are introduced.

4.1. Numerical Solution of RTE

The RTE defines a coupled system of nonlinear integro-differential questions where the unknowns are the monochromatic radiation intensity and the temperature field. There is no known analytical solution to this equation. A finite difference method based on a discretization of the medium is utilized in the solution of RTE. RTE discretization involves three distinct problems: the angular, space, and spectral discretizations [11].

4.1.1. Angular Discretizations

The angular space is divided into m sectors and $\{\mu_j\}_{j=1}^{m}$ denote the discrete angular directions where $0 < \mu_j \leqslant 1$ for $1 \leqslant j \leqslant m/2$ and $\mu_j = -\mu_{m+1-j}$ for $m/2 + 1 \leqslant j \leqslant m$.

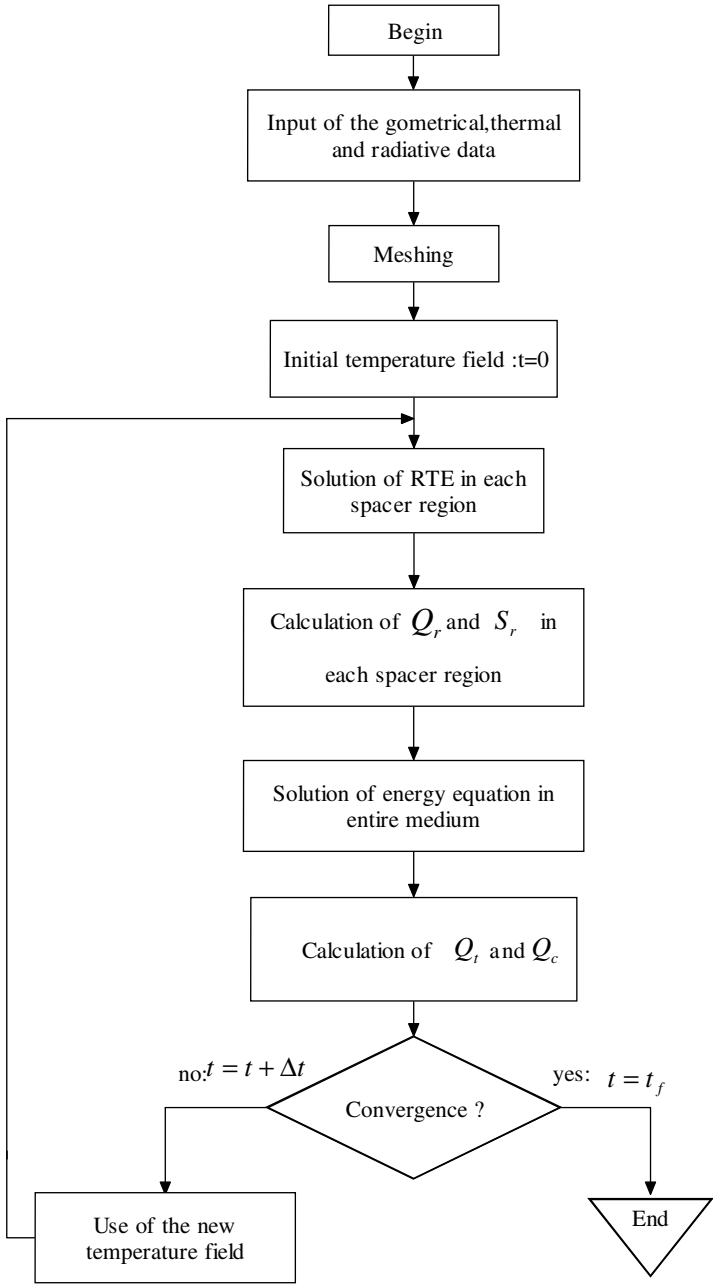

Fig. 5. Flow chart for the solution of coupled equations.

4.1.2. Space Discretizations

The space discretizations with the previous angular discretizations are considered the spatial domain $[0, E_l]$ and are divided into $N_s + 1$ equal intervals of length Δy. A mesh of $N_s + 2$ points between $[0, E_l]$ is considered, so $y_i = i \times \Delta y$ for $0 \leqslant i \leqslant N_s + 1$.

4.1.3. Spectral Discretizations

We also considered the spectral discretizations of RTE, which must be solved for each wavelength λ. For the required resolution, we account for the contribution of all significant wavelengths λ_k $(1 \leqslant k \leqslant N_\lambda)$.

Finally, we need to solve the following discretized set of equations:

$$\begin{aligned}\mu_j \frac{I_{\lambda_k}(y_{i+1}, \mu_j, t) - I_{\lambda_k}(y_{i-1}, \mu_j, t)}{2\Delta y} &= \sigma_{a\lambda_k}(\mu_j) I_{b,\lambda}(T(y_i, t)) - \beta_\lambda(\mu_j) I_{\lambda_k}(y_i, \mu_j, t) \\ &\quad + \sum_{k=1}^{N_\lambda} \sum_{j=1}^{m} C_{\lambda_k, j} I_{\lambda_k}(y_i, \mu_j, t) \end{aligned} \tag{16}$$

where the coefficient $C_{\lambda_k, j}$ takes into account the scattering factors and the integration weights. In this study the integration weights, Φ_λ and $\sigma_{s\lambda}$, are functions of μ and λ. It should be mentioned that $1/c\partial I_\lambda(y, \mu, t)/\partial t$ in Eq. (10) can be neglected due to the large value of c. In this study, $N_\lambda = 211$, $m = 25$, and $N_s = 44$ for the four interior fibrous insulation spacers, and $N_s = 22$ for the two outer fibrous insulation spacers.

4.2. Numerical Solution of Conservation of Energy Equation

In the present study, a finite volume form of the conservation of energy equation is utilized. After discretizing the domain and applying the energy balance to a finite volume, and assuming non-uniform spacing and temperature dependent properties, we get

$$\begin{aligned}&\left(\rho_{i-1} C_{p,i-1} \frac{\Delta y_{i-1}}{2} + \rho_i C_{p,i} \frac{\Delta y_i}{2}\right) \frac{T(y_i, t + \Delta t) - T(y_i, t)}{\Delta t} \\ &= \frac{k\left(T\left(y_{i-1}, t + \Delta t\right)\right)}{\Delta y_{i-1}} \left(T\left(y_{i-1}, t + \Delta t\right) - T(y_i, t + \Delta t)\right) \\ &\quad + \frac{k(T(y_i, t + \Delta t))}{\Delta y_i} \left(T\left(y_{i+1}, t + \Delta t\right) - T(y_i, t + \Delta t)\right) \\ &\quad + S_r(y_i, t + \Delta t) \Delta y_i \end{aligned} \tag{17}$$

The subscript defines the spatial location of the nodes. Equation (17) is the most general form of the governing conservation of energy equation in a finite volume form. When the radiative source term $S_r(y_i, t+\Delta t)$ is known, the energy Eq. (17) can be solved. For this application, Δt is constant and is equal to 0.5 s.

4.3. Iteration Convergence

The convergence criterion for the solution of the coupled system of equations is met when the coupled temperature behavior satisfies the following expression:

$$\max_{1 \leqslant i \leqslant nt} \left| \frac{T(y_i, t+\Delta t) - T(y_i, t)}{T(y_i, t+\Delta t)} \right| \leqslant \varepsilon \tag{18}$$

where ε has a given strictly positive real value. In this application, the convergence criterion is equal to 10^{-6}, namely, $\varepsilon = 10^{-6}$.

5. NUMERICAL RESULTS AND DISCUSSION

In order to evaluate the performance of the MTI and its function as a component of a metallic thermal protection system, the MTI was located between the 3.24 mm thick Inconel plate and an aluminum plate of the same thickness, while the 13.14 mm thick silica insulation with a density of $20\,\mathrm{kg \cdot m^{-3}}$ was installed between the aluminum plate and the water-cooled plate. The silica insulation was made of randomly oriented silica fibers with a diameter of $7\,\mu$m. A schematic of the MTI test installation is shown in Fig. 6. This installation simulated the actual situation of the metallic thermal protection system with MTI at the reentry aerodynamic heating conditions. The Inconel panel served as the hot-side solid boundary, while the aluminum plate represented the launch vehicle structure. The aluminum plate is made of Aluminum-T2024, while the Inconel panel is made of Inconel alloy 718. Thermophysical properties of the Inconel panel and the aluminum plate are given in Ref. 12.

The heat transfer model for the non-gray conditions in this study is compared with that for the gray. They are different in their modeling for radiation heat transfer. To compare numerical results for coupled heat transfer in non-gray MTI with those obtained by the two-flux model, the model using the two-flux method is introduced in the following section.

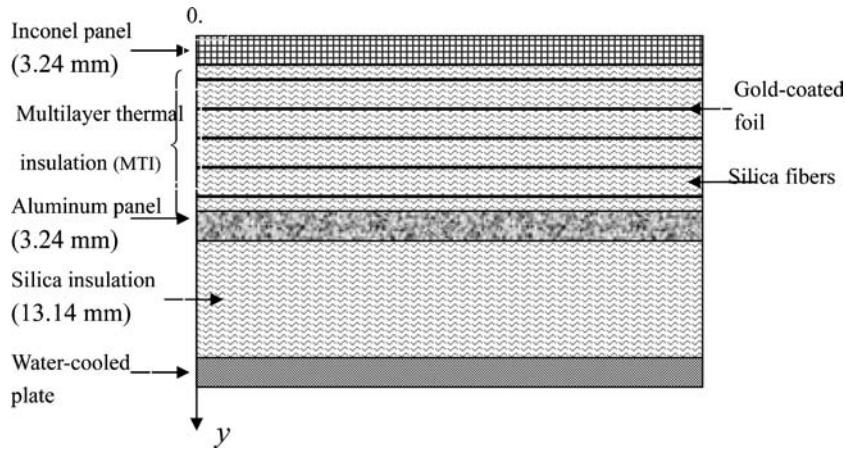

Fig. 6. Schematic of multilayer thermal insulation evaluating installation.

5.1. Introduction of the Model Using the Two-Flux Method

The governing conservation of energy equation for the problem of combined radiation and conduction in a radiation participating media with a thickness E bounded by two solid surfaces at specified temperatures is given in Eqs (1) to (5). The assumptions used in the two-flux formulation consist of isotropic scattering, homogeneous and gray media, and diffuse emitting and reflecting surfaces. The radiant heat flux is given by [12]

$$Q_r(y,t) = -\frac{1}{3\beta}\frac{\partial G(y,t)}{\partial y} \tag{19}$$

where β is the extinction coefficient and G is the incident radiation. The incident radiation in each fibrous spacer is obtained by solving the following second-order differential equation:

$$-\frac{1}{3\beta^2(1-\omega)}\frac{\partial^2 G(y,t)}{\partial y^2} + G(y,t) = 4\sigma T^4(y,t) \tag{20}$$

where ω is the scattering albedo, defined as the ratio of the scattering coefficient and extinction coefficient. This is subject to the following boundary conditions at the bounding surfaces for the fibrous spacers, or at two foils, or at a foil and solid bounding surface:

$$-\frac{2}{3\beta\left(\frac{\varepsilon_L}{2-\varepsilon_L}\right)}\frac{\partial G(y_L,t)}{\partial y}+G(y_L,t)=4\sigma T^4(y_L,t) \tag{21}$$

$$\frac{2}{3\beta\left(\frac{\varepsilon_R}{2-\varepsilon_R}\right)}\frac{\partial G(y_R,t)}{\partial y}+G(y_R,t)=4\sigma T^4(y_R,t) \tag{22}$$

where ε is the emissivity of a foil or a solid bounding surface, σ is the Stefan-Boltzmann constant, and the subscripts L and R refer to the fibrous spacers' two bounding surfaces. Eqs (1) to (5) and Eqs (19) to (22) provide the governing equations and the most general form of the boundary conditions and initial conditions for the numerical heat transfer model.

For comparison of the results obtained for non-gray fibrous insulation with those of assumed gray fibrous insulation by appropriate numerical models, the silica fibrous insulation is assumed to be grey. The two-flux method can be used for the fibrous insulation assuming gray media. The two parameters of the two-flux approximation, the extinction coefficient β and the scattering albedo ω for the silica fibrous insulation, must be evaluated. They are average values and are determined by [2, 9, 13]

$$\beta=\int_{\lambda_{\min}}^{\lambda_{\max}}\beta_\lambda d\lambda \Big/ (\lambda_{\max}-\lambda_{\min}) \tag{23}$$

$$\omega=\int_{\lambda_{\min}}^{\lambda_{\max}}\sigma_{s\lambda}d\lambda \Big/ \int_{\lambda_{\min}}^{\lambda_{\max}}\beta_\lambda d\lambda \tag{24}$$

5.2. Steady-State Results

For obtaining the steady-state calculated results, the numerical solution was advanced in time until steady-state conditions were achieved. At steady state, the effective thermal conductivity was calculated from Fourier's law of heat conduction using the calculated total steady-state heat flux (including both radiative and conductive heat fluxes) and the imposed temperature difference across the MTI. The comparison of results obtained using the numerical model in this study and those obtained using the two-flux model effective thermal conductivities for the multilayer sample is shown in Fig. 7.

In simulating steady-state coupled heat transfer in multilayer insulation using the numerical model, the simulated Inconel panel and water-cooled plate temperatures were used for the boundary conditions. At steady state, a comparison of temperature profiles vs. depth for the multilayer sample obtained using the numerical model in this study and

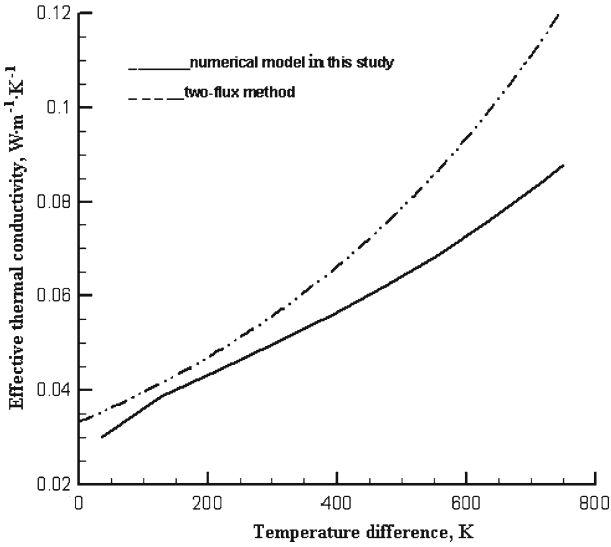

Fig. 7. Comparison of numerical model in this study and two-flux model for effective thermal conductivity of multilayer insulation.

obtained using the two-flux model is shown in Fig. 8. As shown in Figs 7 and 8, the difference is obvious, especially at high temperature. Compared with the effective thermal conductivities and temperature profiles vs. depth obtained using the two-flux model, the predictions using the numerical model in this study are higher by a maximum of 23.7% and 7.9%, respectively.

5.3. Transient Results

In simulating the transient coupled heat transfer in multilayer insulation using the numerical model, the simulated temporal variations of the Inconel panel and water-cooled plate temperature were used for the boundary conditions. The temporal variations of the Inconel panel temperature that could be achieved in simulating re-entry conditions are shown in Fig. 9, along with the corresponding desired radiation equilibrium temperature for typical re-entry profiles. The water-cooled plate temperature was maintained around room temperature (300 K). The predictions from the numerical model of this study and those obtained by using the two-flux formulation temperatures of the aluminum panel and one point of the multilayer insulation (distance from bottom of the Inconel panel is 16.38 mm) are shown in Fig. 9. At times less than 1000 s,

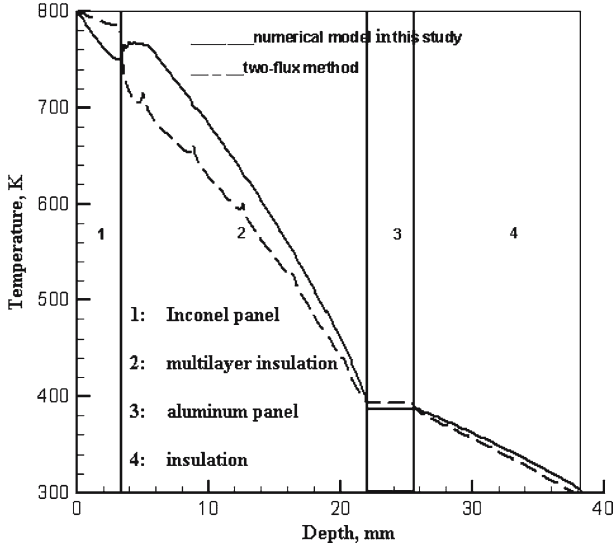

Fig. 8. Comparison of numerical model in this study and two-flux model for temperature profiles vs. depth at steady state.

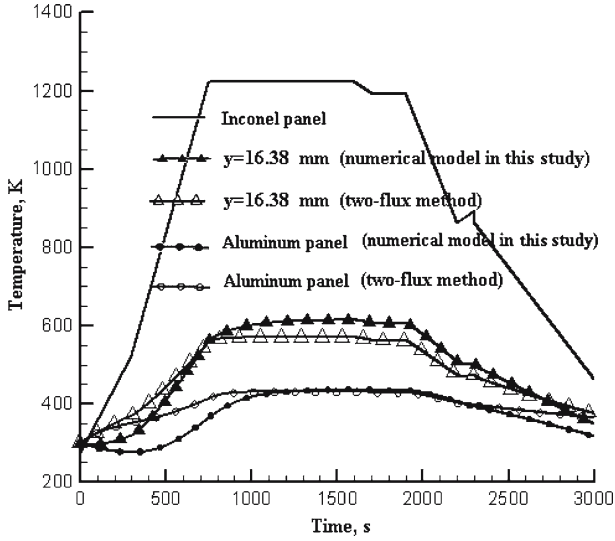

Fig. 9. Comparison of numerical model of this study and two-flux model for transient multilayer insulation.

when the Inconel panel temperature increases with a large gradient, the difference between the temperature of the aluminum panel obtained with the numerical model in this study and the two-flux numerical model is enormous, but the temperature obtained with the numerical model of this study is lower. However, between 1000 and 2500 s the temperature of the aluminum panel obtained with the numerical model of this study is higher than that obtained with the two-flux formulation, and the difference still is large.

As shown in Fig. 9, the difference between the aluminum panel's temperature predicted by using the numerical model in this study and that obtained by using the two-flux formulation has an average value of 19.25 K (the former is 455.55 K and the latter is 436.30 K; and the highest temperatures are 458.25 K and 437.35 K, respectively), which shows that if a non-gray fibrous layer is treated as a gray medium in the metallic thermal protection system, it will give unreliable results in insulation design.

6. OPTIMIZATION OF MTI

The theoretical model was developed to optimize the design of the MTI. The model parameters include the emissivity of the foils, the number of screens and their locations, the spacer material, the thickness of the spacer material, and the total thickness of the insulation as well as the maximum temperature of the insulation surface. If the fibrous spacer is optically thick, the reflectance of the foils will not have any appreciable effect on the overall radiation heat transfer. Therefore, except for the distance between the screens, the effect of the emissivity of the foils on the effective thermal conductivity of the MTI should be considered. In this section, results about the optimum MTI configuration, i.e., the emissivity of the foils and their locations, are discussed in order to obtain simple design rules. The multilayer insulation discussed above has been employed again; however, only the gold-coated foils have been replaced with the various metal-coated ceramic substrate foils in order to investigate the effect of the emissivity of the foils on the effective thermal conductivity of the MTI. In the present discussion, a numerical experiment refers to a numerical solution of the governing heat transfer equations for the thermal design problem described in the previous section using model parameters. For each set of numerical experimental conditions, the emissivity of the foils is variable, while other model parameters are constant. The temperatures of the Inconel panel and water-cooled plate were used for the boundary conditions, which were 800 and 300 K, respectively. The numerical solution was advanced in time until steady-state conditions were achieved. The relationship between the number of foils and their locations

Table I. Relationship between Number of Foils and Their Locations

Number of Foils	1	2	3	4	5
Location of Foils (distance from the bottom of Inconel panel, mm)	1.8	5.62	9.44	13.26	15.10

Table II. Results of Design of Experiment Analysis

Trial number	Emissivity of foils					Temperature of aluminum panel (K)
	Foil 1	Foil 2	Foil 3	Foil 4	Foil 5	
1	0.1	0.6	0.6	0.6	0.1	386.54
2	0.1	0.6	0.6	0.6	0.2	378.69
3	0.1	0.6	0.6	0.6	0.6	374.98

is shown in Table I. The effect of the emissivity of the foils on the temperature of the aluminum panel is reported in Table II.

A comparison of trials 1, 2, and 3 shows that the temperature of the aluminum panel near the steel alloy-coated foil ($\varepsilon = 0.6$) is the lowest while the temperature of the aluminum panel near the gold-coated foil ($\varepsilon = 0.1$) is the highest, and the temperature of the aluminum panel near the ceramic foil ($\varepsilon = 0.2$) falls between these two values. This is due to the absorption and re-emission properties of the foils, namely, foils with a higher reflectance (lower emissivity) have a stronger effect on the aluminum panel than foils with a lower reflectance with the same temperature in an optically thick space.

The cost of the gold-coated reflective foils is extremely high compared to the cost of the steel alloy-coated foils and silica fibrous insulation. Therefore, the present numerical experiment can be used in future studies to provide insights regarding the costs and benefits of the MTI.

7. CONCLUDING REMARKS

(a) A numerical model developed for modeling the transient coupled radiative and conductive heat transfer in the MTI which consists of non-gray semitransparent materials and reflective foils is investigated for metallic thermal protection systems subjected to re-entry aerodynamic

heating. The numerical result is compared with the numerical result obtained from the two-flux method for gray materials. It was found that the effective thermal conductivities predicted in this study are larger than those obtained by using the two-flux formulation, which shows that if a numerical model for gray media is used for non-gray media, it could give less heat flux than it should, and as a consequence, may cause design problems and subsequent equipment failure.

(b) A numerical model is used to determine the optimum design specifications for multilayer insulation subjected to re-entry aerodynamic heating. It was found that the use of a steel alloy-coated foil ($\varepsilon = 0.6$) near a cooler aluminum panel would result in an effective insulation design.

REFERENCES

1. K. Daryabeigi, *Proc. 35th AIAA Thermophys. Conf., AIAA 2001-2834*, Anaheim, California (2001), p. 10.
2. W. W. Yuen, *Proc. The 6th ASME-JSME Thermal Engineering Joint Conf.*, *TED-AJ03-126*, Hawaii Island, Hawaii (2003), p. 201.
3. S. V. Reznik, W. P. P. Fisher, D. Martines, L. Ya. Paderin, N. V. Pavlyukevich,e D. Petit, and P. V. Prosuntsova, *J. Eng. Phys. Thermophys.* **77**:3 (2004).
4. David Lacroix, Gilles Parent, Fatmir Asllanaj, and Gérard Jeandel, *J. Quant. Spectrosc. Radiat. Transfer* **75**:589 (2002).
5. Fatmir Asllanaj, *Proc. Eurotherm73 on Computational Thermal Radiation in Participating Media*, Mons, Belgium (2003), p.193.
6. C. Langlais and S. Klarsfeld, *Journée d'étude du groupement universitaire de thermique* **6**:19 (1985).
7. M. F. Modest, *Radiative Heat Transfer*, Mech. Eng. Series (McGraw-Hill: New York, 1993), p. 303.
8. J. H. Joseph, W. J. Wjiscombe, and J. A. Weinman, *J. Atmos. Sciences* **33**:2452 (1976).
9. T. Sghaier, B. Cherif, and M. S. Sifaoui, *J. Quant. Spectrosc. Radiat. Transfer* **75**:257 (2002).
10. E. M. Sparrow and R. D. Cess, *Radiat. Heat Transfer*, Augmented Ed. (McGraw-Hill, New York, 1978), pp. 91, 92.
11. F. Asllanaj, A. Milandri, G. Jeandel, and J. R. Roche, *Int. J. Numer. Methods Eng.* **54**:1649 (2002).
12. Kamran Daryabeigi, *Design of High Temperature Multi-layer insulation for Re-entry Launch Vehicles* (Ph. D. Dissertation, University of Virginia, 2000), pp. 27, 28.
13. J. F. Sacadura and D. Baillis, *Rev. Gen. Therm.* **41**:699 (2002).